Supporting Online Material for

Electric Fields at the Active Site of an Enzyme: Direct Comparison of Experiment with Theory

Ian T. Suydam, Christopher D. Snow, Vijay S. Pande, Steven G. Boxer*

*To whom correspondence should be addressed. E-mail: sboxer@stanford.edu

Published 14 July, *Science* **313**, 200 (2006)
DOI: 10.1126/science.1127159

This PDF file includes:

Other Supporting Online Material for this manuscript includes the following:
(available at www.sciencemag.org/cgi/content/full/313/5784/200/DC1)

Databases S1 to S3 as zipped archives

Supporting Online Material

Electric Fields at the Active Site of an Enzyme:

Direct Comparison of Experiment with Theory

Ian T. Suydam, Christopher D. Snow, Vijay S. Pande and

*Steven G. Boxer**

Department of Chemistry

Stanford University

Stanford, California 94305-5080

sboxer@stanford.edu

650-723-4482

Table of Contents

Material and Methods

Vibrational Stark Spectra. The vibrational Stark spectrum of IDD743 was obtained as previously described (*S1*). Briefly, a 150 mM solution was prepared in 2-Me THF and filled into a sample cell consisting of two sapphire windows, each coated with approximately 50 Å nickel semi-transparent electrodes and separated by a 30 μm Teflon spacer. The sample was cooled rapidly to 74 K in a liquid nitrogen immersion cryostat (*S2*) producing an optical quality glass. Spectra were obtained using a Bruker 66V/S FTIR system with a nitrogen cooled Indium Antimonide detector at 1.0 cm^{-1} resolution. Unpolarized light was used and the external electric field was applied perpendicular to the oscillating electric field of the infrared beam ($\chi = 90°$). For field-on spectra, up to 1,500 volts were applied across the sample producing a field of 0.5 MV/cm. The field was cycled on and off between interferograms until a total of 256 field-on and 256 field-off interferograms had been collected.

A Stark spectrum is defined as the difference between the field-on and field-off absorption spectrum, $\Delta A = A(F_{ext}) - A(F = 0)$. For isotropic samples the Stark spectrum can be fit to the sum of the frequency-weighted derivatives of the zero-field absorption spectrum (*S1*) (Eq. S1),

$$\Delta A_\chi(\bar{\nu}) = |F|^2 A_\chi A(\bar{\nu}) + \frac{|F|^2}{15hc} B_\chi \bar{\nu} \frac{\partial}{\partial \bar{\nu}} \frac{A(\bar{\nu})}{\bar{\nu}} + \frac{|F|^2}{30h^2c^2} C_\chi \bar{\nu} \frac{\partial^2}{\partial \bar{\nu}^2} \frac{A(\bar{\nu})}{\bar{\nu}} \qquad \text{(S1)}$$

where F is the applied field, and A_χ, B_χ, and C_χ are the zeroth, first and second derivative contributions to the fit. For 1 dimensional vibrational modes such as mononitriles, $\Delta\vec{\mu}$ lies along the transition dipole moment of the vibration ($\zeta = 0°$) which is expected to lie

along the bond vector (*S3*). With χ set to 90°, the magnitude of $\Delta\vec{\mu}$ can be obtained directly from the second derivative contribution to the fit (*S1*) (Eq. S2).

$$|\Delta\mu| = \left(\frac{C_\chi}{3}\right)^{1/2} \qquad \text{(S2)}$$

Because sample molecules experience a field that is dependent on local solvent structure, the applied field cannot be calculated simply from the applied voltage, electrode spacing and bulk dielectric. For this reason properties derived from Stark data are often expressed in terms of a local field correction factor, f , where $F_{local} = fF_{ext}$ (the local field correction is, in general, a tensor quantity, approximated here as a scalar). There are various ways of approximating f, and we have previously estimated its value to be 1.1 for samples in frozen 2-Me THF (*S3*).

Fig. S1 shows the absorption spectrum, vibrational Stark spectrum and derivative contributions for the nitrile vibration of IDD743 in 2-Me THF. The magnitude of the change in dipole moment was obtained from the second derivative contribution to the Stark fit which yielded $f\left|\Delta\mu_{probe}\right|$ = 0.76 cm^{-1}/(MV/cm), or 0.045 D. This value is consistent with that obtained for other aromatic nitriles (*S1, S4*) and is a moderately large sensitivity within this bond type. We have previously shown that $\Delta\vec{\mu}$ lies along the CN bond for mononitriles and points from the nitrile nitrogen to the nitrile carbon (*S3*). If we define the molecular axis as pointing from the nitrile carbon to the nitrile nitrogen and use f = 1.1, then $\Delta\vec{\mu}_{probe}/hc$ = -0.69 cm^{-1}/(MV/cm). Based upon this calibration, a

change in field along the CN bond of 1.0 MV/cm is expected to shift the nitrile stretching frequency by + 0.69 cm^{-1} (Eq. 1, main text).

Mutagenesis. The gene for wild-type human aldose reductase was obtained from Alberto Podjarny in the pET-15b expression vector (Novagen). Mutagenesis was carried out using the QuickChange® site-directed mutagenesis kit (Stratagene) following the manufacture's protocol, and primers were designed to meet the manufacture's guidelines. The genes for wild-type and each mutant were resequenced to confirm the expected changes.

Protein Expression and Purification. Expression and purification of hARL2 was similar to that previously reported (*S5*). All plasmids were transformed into BL21(DE3) *E. coli* (Novagen). Cells were grown in 4 liter fermentations in media containing 11 g tryptone, 22.5 g yeast extract, 10.9 g K_2HPO_4, 3.6 g KH_2PO_4, 20 g glucose and 100 mg ampicillin per liter at 37 °C. The pH of the media was maintained at 7.0 by the addition of ammonium hydroxide. At an optical density of 0.8 protein expression was induced by the addition of 1 mM IPTG. The cells were then pelleted, resuspended and lysed with a cell homogenizer operating between 15-20 kpsi. After removing cell debris the lysate was loaded onto a Ni-NTA agarose column and the His-tagged protein was purified following the manufacture's procedure (Qiagen) with an imidazole gradient. The protein was then exchanged into thrombin cleavage buffer (20 mM Tris pH=8.0, 150 mM NaCl, 2.5 mM $CaCl_2$), and thrombin from human plasma was added (2 units thrombin per mg His-tagged protein). The thrombin cleavage reaction was left at room temperature in the dark for 12 hours and then exchanged into 20 mM

Tris, pH = 8.0. Thrombin cleaved protein was loaded onto a 1 ml HiTrap Q HP anion exchange column (Amersham) and eluted with a step gradient to 80 mM NaCl. The purity of each protein sample was confirmed by polyacrylamide gel electrophoresis and by mass spectrometry. For each mutant a mass spectrum corresponding to a single protein species was observed with a mass matching the expected GSHM-hALR2 sequence within the resolution of the instrument (~ 7 Da). Typical yields were in the range of 20-50 mg purified protein per liter of media.

Enzyme Kinetics. All kinetic measurements were performed with DL-glyceraldehyde as substrate and NADPH as cofactor. Reactions were performed in 1.0 ml phosphate buffer, pH = 7.0 at room temperature. Initial rates were measured by following the decrease in NADPH absorption at 340 nm. Typical reactions contained 100 μM NADPH, 100-500 nM enzyme and DL-glyceraldehyde concentrations between 5-200 μM. Kinetic constants were obtained by measuring initial rates for at least eight substrate concentrations in triplicate and fitting the result directly to the Michaelis-Menten function. Kinetic constants were determined for mutants not previously described (Table S1). It has been noted that oxidation of Cys298 can produce enzymes with enhanced activity (*S6*). The mass spectra we obtained for each mutant were consistent with unoxidized proteins, and the kinetic constants we obtained for wild-type were very similar to those reported (*S7*). With the exception of V47D the catalytic efficiency of these mutants is comparable to wild-type. The significant drop in k_{cat} for V47D is likely due to its proximity to Tyr48, which acts as the proton donor for the reaction (*S8*) and whose pK_a is perturbed toward neutrality in wild-type hALR2 (*S9*).

Circular Dichroism Spectra. For those mutants that are catalytically inactive, circular dichroism spectra were obtained. All circular dichroism spectra were obtained at room temperature with an AVIV 202 spectrometer from 185-207 nm at 2.0 nm resolution. Solutions were 10 μM enzyme in phosphate buffer, pH = 7.0. These spectra were very similar to wild-type and matched those previously reported (*S8*) (data not shown).

Infrared Absorption Spectra. Infrared absorption spectra of IDD743 bound to wild-type and mutant hALR2 enzymes were obtained in liquid solution at room temperature. Samples were prepared by adding 1 equivalent of IDD743 and 1 equivalent $NADP^+$ to purified enzyme in phosphate buffer, pH = 7.0. Samples were initially prepared between 50-100 μM and then concentrated to 1-2 mM using ultrafiltration membranes with a cut off of 10 kDa. Concentrating samples after the addition of IDD743 ensured that any unbound inhibitor was removed from protein samples before infrared spectra were obtained. Concentrated samples were loaded into a liquid infrared cell constructed of two sapphire windows separated by two Teflon spacers. Spacers of different thickness were chosen to help minimize fringes caused by reflections between the two windows (typically one 75 μm spacer and one 100 μm spacer). Background samples were either identical protein solutions without IDD743 added or buffer solution (the holoenzyme absorbs minimally between 2200-2300 cm^{-1}, and identical results were obtained with protein or buffer background). Spectra were obtained using either a Bruker 66V/S, or Bruker Vertex 70 FTIR spectrometer with a cooled Indium Antimonide detector at 0.5 cm^{-1} resolution. Absorption maxima in the nitrile region were in the range

of $1x10^{-3}$ to $4x10^{-3}$, consistent with a 1:1 complex between IDD743 and hALR2 mutants and the measured extinction coefficient of the nitrile absorption (200 $M^{-1}cm^{-1}$). Because water absorbs strongly in the 2200-2300 cm^{-1} region for the path lengths used an imperfect baseline was observed for all absorption spectra. Baselines were corrected by fitting a polynomial through points away from the nitrile absorption. Peak frequencies were obtained by fitting the average of at least three independently obtained absorption spectra. Table S2 summarizes nitrile stretching frequencies and spectral shifts relative to wild-type for IDD743 bound to the eight mutants studied.

Wild-Type hALR2/$NADP^+$/IDD743 Model. There are currently no structures available for hALR2 with the inhibitor IDD743 bound. However, two closely related inhibitors, IDD393 and IDD594 (Fig. 1C), have been crystallized with wild-type hALR2/$NADP^+$ and solved to high resolution (1.0 Å for the IDD393 structure (*S11*) and 0.66 Å for the IDD594 structure (*S12*)). We constructed a model for wild-type hALR2/$NADP^+$/IDD743 based on these structures. From the IDD393 structure we modified the inhibitor, substituting fluorine for chlorine and adjusting the bond length to 1.32 Å. A nitrile was then added at the adjacent carbon with a C-C distance of 1.44 Å and a C-N distance of 1.14 Å. As with the published IDD594 structure the IDD393 structure is of sufficient resolution to assign multiple conformations to several residues. We selected the A conformation at all residues. Only six residues within 10 Å of the IDD743 nitrile are assigned two conformations in the IDD393 structure (H46, Q49, F121, D216, C298, L300). The alternative conformation for each of these residues is very similar to the dominant conformation. The IDD393 structure also contains 1,106 water

molecules, thirteen of which have B-factors below 10 $Å^2$. We removed all water molecules including HOH 3002 which bridges ND1 of His 110 and the backbone carbonyl of Lys^{77} and is 9.2 Å from IDD743's nitrile.

Hydrogens were added to the inhibitor and cofactor to conform to standard lengths and geometries. The carboxylate of IDD743 was left unprotonated as is suggested in the IDD594 crystal structure and by inhibition studies on carboxylate containing inhibitors of hALR2 (*S13*). The 2′ phosphate of $NADP^+$ was also left unprotonated due to its proximity to Lys^{262}. Hydrogens were added to protein atoms with the program Molprobity (*S14*). All Cys and Tyr residues were left neutral while Arg and Lys residues were fully protonated and Glu and Asp residues were deprotonated. All His residues were left neutral and protonated at ND1 or NE2 based on probable hydrogen bonding patterns (ND1 for residues 41, 46 and 163, NE2 for residues 83, 110, 187, 240, 306 and 312). The 0.66 Å resolution structure of IDD594 bound to hALR2 assigns over 50% of the protein's hydrogens. We used the F_0-F_c density map from the IDD594 structure to confirm the protonation states and orientations of our model, most importantly the assignment of His^{110} as singly protonated at NE2 and the orientation of the Tyr^{48} hydroxyl hydrogen, both of which are within 10 Å of IDD743's nitrile. The protonation state of this model also conforms to that used by Lecomte and coworkers who have performed continuum electrostatic and DFT calculations on the active site of the IDD594 structure (*S15*).

Mutant Models. Mutant pdb structures were created with the program PyMol (*S16*) using the mutagenesis tool. This program ranks possible side chain conformations

by the frequency the conformation is reported in the protein databank. Side chain conformations were selected by accepting the most frequently observed conformation that did not bring nonbonded atoms within their van der Waals radii. Potential mutants for infrared studies were created in four groups. The first group contained mutations that have been previously reported in the literature and that might be expected to alter the field at the nitrile of IDD743. The second group was constructed by aligning the crystal structures for human aldose reductase (hALR2) and human aldehyde reductase (hALR1). The tertiary fold of these enzymes is remarkably similar and the location of many side chains in the active site is nearly identical (*S12, S17*). We selected residues within 10 Å of the inhibitor in the IDD393 structure that are not structurally conserved between the enzymes and mutated them to the hALR1 residue. Side chain conformations were selected to match those observed in the hALR1 structure. The third group of mutations replaces all charged residues within 15 Å of IDD743's nitrile to alanine. The fourth group mutates side chains that are within 10 Å of IDD743's nitrile but excludes side chains that make important contacts with the inhibitor (W20, K21, Y48, H110, W111, T113, F122, P123, P218, W219, A299, and L300). The remaining sites were mutated to all possible amino acids that could be accommodated. Ionizable side chains in all groups were protonated based on their unperturbed pK_a with histidine and cysteine residues neutral.

Continuum Electrostatics Calculations. Electrostatic potentials and fields were calculated using DelPhi v.4 (*S18*). This program reads in atomic coordinates, charges, and radii and solves the Poisson-Boltzmann equation with the finite difference method

(*S19*). Charges and radii for protein atoms were taken from the PARSE parameter set last modified in 1994 (*S20*). To complete the parameter set charges and radii for IDD743 and $NADP^+$ were added. Charges for $NADP^+$ were taken from those developed by Ryde and coworkers for molecular mechanics simulations (*S21*). These charges correspond to $NADP^+$ with a charge of -3 (unprotonated 2′ phosphate). Charges for the inhibitor were obtained by calculating the Merz-Kollman charges for IDD743 with the program Gaussian (*S22*). Bond angles and torsions of IDD743 were fixed to those observed in the IDD393 crystal structure but bond lengths were free to optimize. Molecular orbitals were calculated with the Hartree-Fock basis set HF/6-31+(d). For both $NADP^+$ and IDD743 radii were estimated by analogy to atoms found in the PARSE parameter set. Fig. S2 provides a key to atom names for IDD743 and $NADP^+$ in the charge and radii files used (available for download from the supporting online material website).

The contribution to the electric potentials and fields at the nitrile from the nitrile-containing ring of IDD743 are expected to be large and independent of the fields produced from the surrounding protein. Furthermore, calculating potentials and fields with the inhibitor fully charged leads to very large (and physically meaningless) electric fields at the nitrile midpoint, and introduces large errors in the calculated field due to the distribution of the nitrile charges (and neighboring atom centers) onto lattice points in the finite difference method. To eliminate this error we set the charges of all atoms on the nitrile ring of IDD743 to zero for DelPhi calculations. Charges were retained for the remaining inhibitor atoms to include the effect of conformational flexibility in the rest of the inhibitor. Because electric fields were calculated at a single location we employed

overfocusing to minimize grid artifacts. An initial calculation that included the entire system was used to calculate potentials with a coarse grid spacing (0.75 grid $Å^{-1}$, 65 grid lattice). These initial potentials were then used as the boundary condition for a calculation with doubled grid spacing that included one eighth of the system. The process was repeated three times to achieve a grid spacing of 0.167 Å, with the lattice centered on the nitrile midpoint. This routine allowed calculations with fine grid spacings to be completed rapidly enough to perform the calculation on all structures (~250,000) obtained from MD simulations with two values of internal dielectric (ϵ=2 and ϵ=4). The continuum electrostatics calculations required ~60 CPU days on 2.8 GHz Xeon CPUs.

DelPhi Calculations on Potential Mutants. The calculated change in field along the IDD743 nitrile between each potential mutant and wild-type is summarized in Table S3. The most striking result from these calculations is how few mutations were predicted to produce large changes in field along the nitrile bond, even when charged or polar groups are added or removed near the inhibitor nitrile. Many of these mutations are predicted to produce large changes in field at other sites on the inhibitor or in other directions at the nitrile. Less solvated probes may respond more dramatically to mutation. Mutations selected for infrared experiments are shown in bold.

Molecular Dynamics Simulations: Molecular Dynamics (MD) simulations were performed on the wild-type hALR2/$NADP^+$/IDD743 structure and the eight mutant structures used for infrared measurements. MD simulations were carried out with the program TINKER using the OPLS united atom (UA) parameter set (*S23, S24*). This

parameter set reduces the number of atoms in the system by grouping aliphatic hydrogens with the corresponding carbons but treating hydrogens on polar atoms or aromatic carbons explicitly. The removal of aliphatic hydrogens is consistent with the subsequent DelPhi calculations since these hydrogens are assigned a van der Waals radius of zero in the PARSE 94 parameter set. $NADP^+$ and IDD743 were added to the OPLS-UA force field by assigning the same charges as for DelPhi calculations, but with all inhibitor atoms charged. Bond length, angle, and dihedral minima were set to those of our wild-type model for hALR2/$NADP^+$/IDD743. The atom types and the bond stretching, bending and torsion penalties were assigned by analogy to those present in the OPLS-UA set and to favor the initial native ligand conformation. Our modifications to the OPLS-UA parameter set are available for download from the supporting online materials website. Each initial model was energy minimized and used as the starting structure for 50 independent MD trajectories. The MD used the TINKER implementation of Langevin dynamics (a stochastic integrator). Solvent was represented using the Still model of the Generalized Born treatment (*S25*). Each simulation was run independently at 298K (the longest trajectories reach 500 ps). These trajectories were calculated in pieces with the distributed computing project Folding@Home (*S26*) and coordinate structures from the simulations were saved every 0.5 ps. For the V47N mutation five additional minimized starting structures were constructed and ensembles were simulated to identify the preferred conformer for the side chain amide. For each of the five ensembles, conformations with Asn^{47} χ_2 greater than 65 degrees dominated at long time. Because the relaxation of the V47N side chain to the preferred conformation was slow for some initial

structures an initial structure with $\chi_2 > 65$ degrees was chosen to compute average values of field as a function of time (see below). The MD simulations required ~1,000 CPU days on the heterogeneous Folding@Home cluster.

DelPhi Calculations Along MD Generated Trajectories. DelPhi calculations were performed on each of the ~250,000 MD generated structures as described above, with an internal dielectric of 2 and 4. The ensemble averaged relaxation in the electric field was generated by averaging the calculated field for all structures of a given mutant at a given time point (see Fig. S3). For all of the characterized mutations, most relaxation in calculated field occurred within 200 ps. Distributions of field past 200 ps were calculated from at least 2,000 MD generated structures past this time and the means of these distributions were used to calculate the change in field between each mutant and wild-type, with an internal dielectric of 2 (Fig. S4) and 4. Mean values of field calculated with an internal dielectric of 2 better matched the expected frequency/field correlation (Fig. 4). This is consistent with previous results, because an internal dielectric between 4-6 is typically used for single point calculations, where the continuum model is used to implicitly model conformational flexibility (*S27*). Having modeled this flexibility explicitly with MD simulation we would expect the best correlation with an internal dielectric that accounts for electronic polarizability only, and this is observed.

Figures and Legends

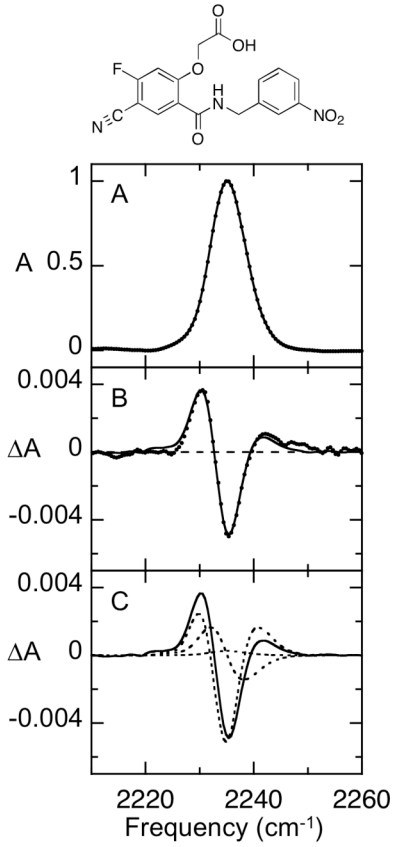

Fig. S1. Absorption and vibrational Stark spectrum of IDD743 in the nitrile stretching region. **(A)** Absorption spectrum scaled to an absorption maximum of 1.0. **(B)** Stark spectrum (field on - field off) scaled to an absorption maximum of 1.0 and an applied field strength of 1.0 MV/cm. Dots represent the data, solid line represents the fit through the data, and dashed line represents $\Delta A = 0$. **(C)** Solid line is fit to data from panel B, dashed lines are the zeroth, first, and second derivative contributions to the fit (Eq. S1).

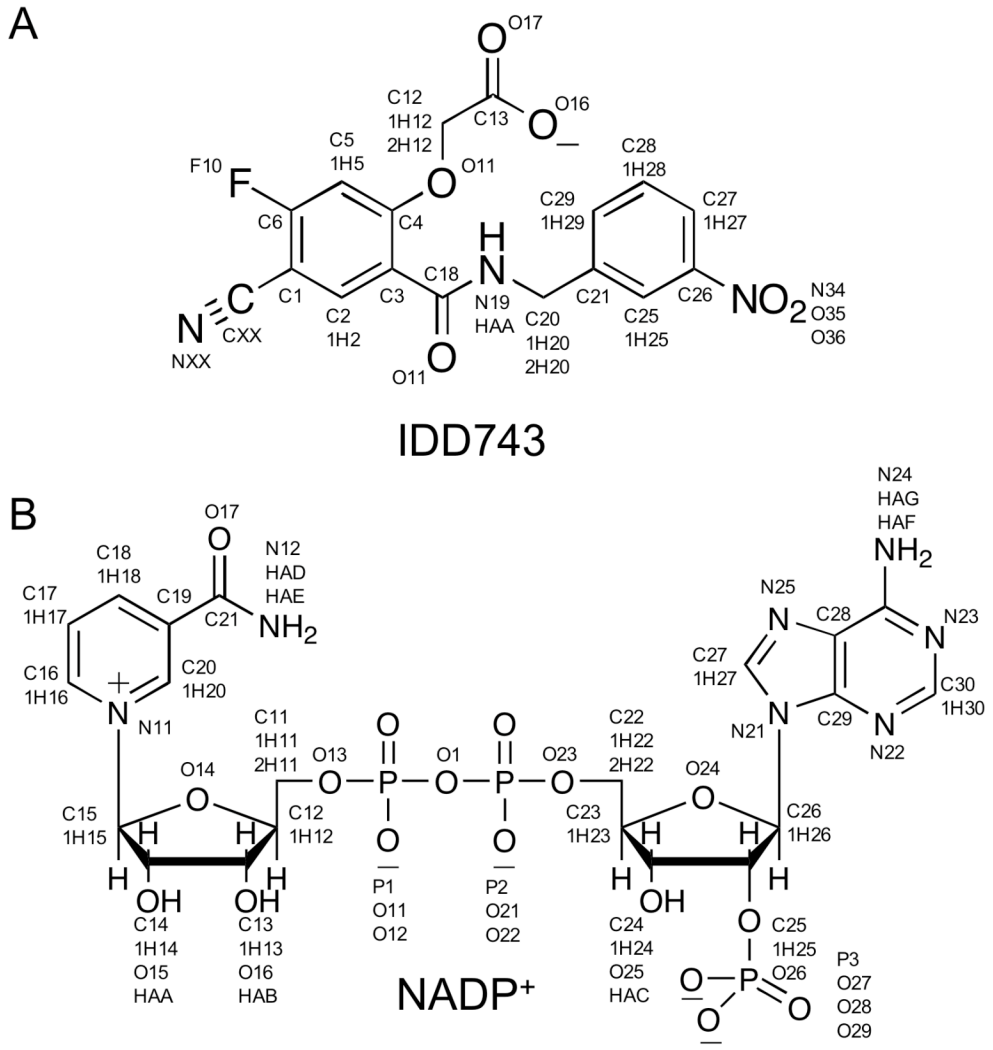

Fig. S2. Atom names for IDD743 **(A)** and $NADP^+$ **(B)**.

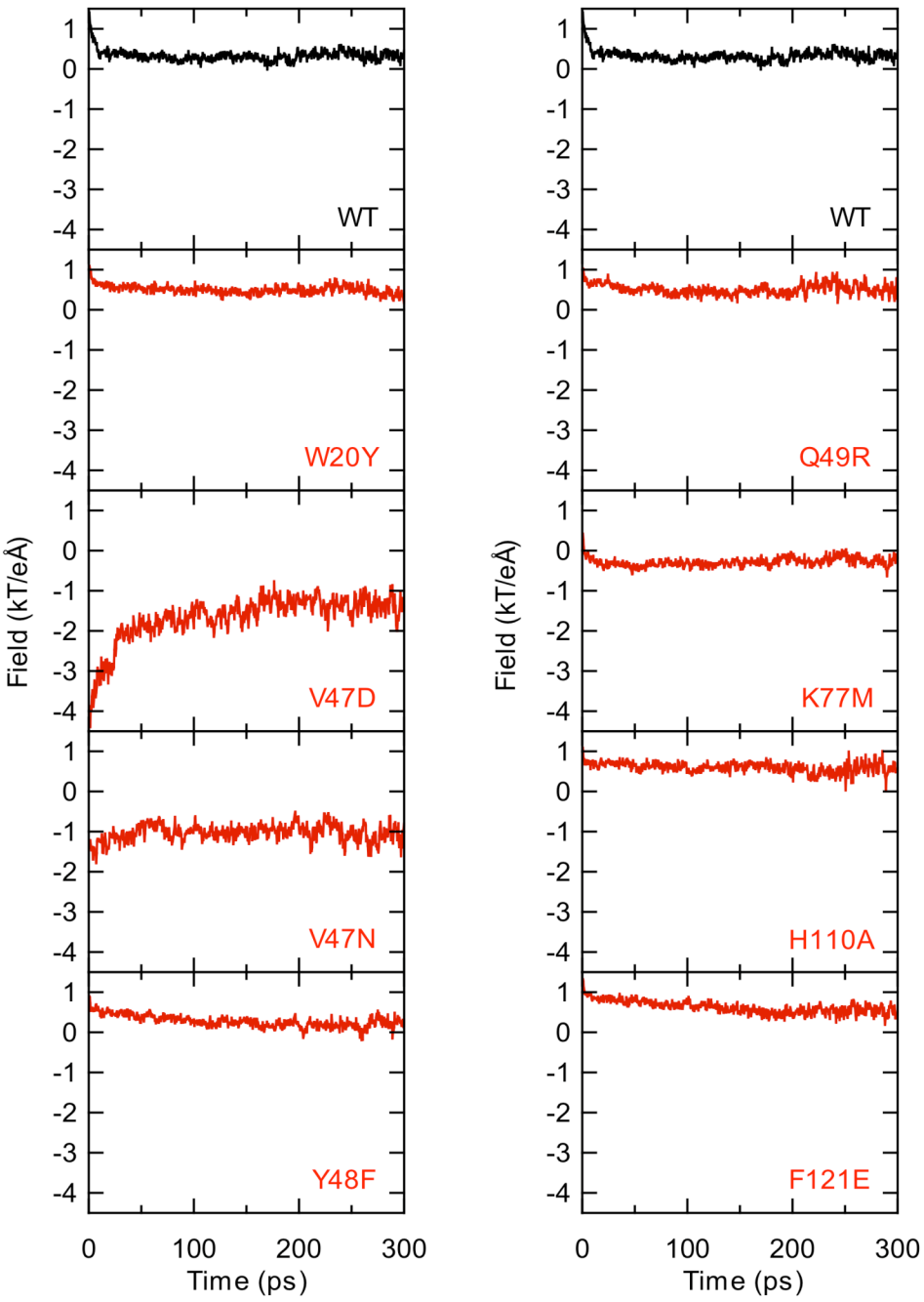

Fig. S3. Average projection of field along the nitrile of IDD743 calculated from multiple trajectories at each time point with INDI =2.

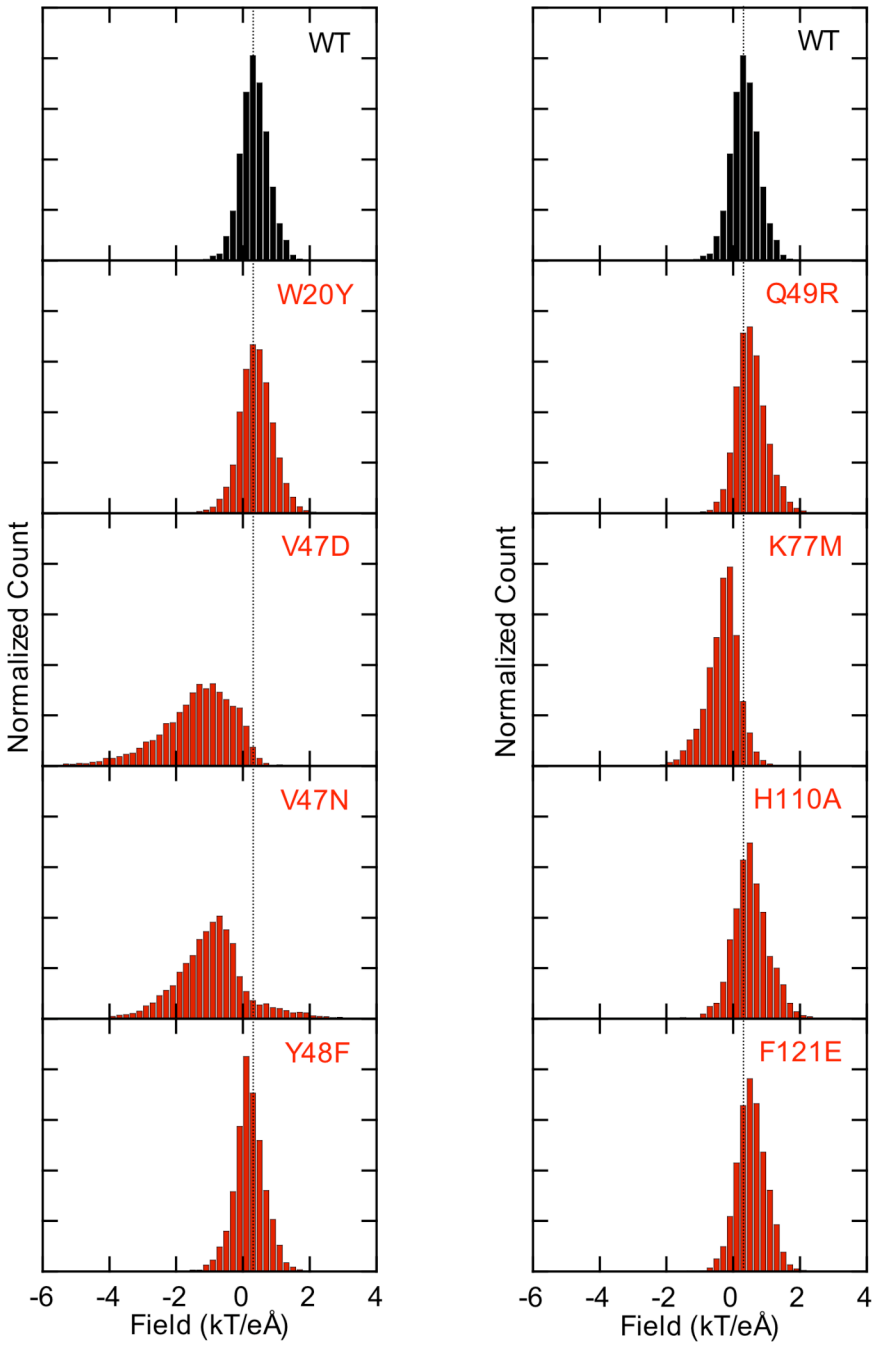

Fig. S4. Distribution of electric fields along the nitrile of IDD743 for time points past 200 ps with INDI=2. Dashed line shows mean value of the wild-type distribution.

Tables and Legends

Table S1: Apparent kinetic constants for the hALR2 mutants studied[a]

	k_{cat} (s^{-1})	K_m (μM)	k_{cat}/K_m (s^{-1}/ M)
wild-type[b]	0.45	20	22687
W20Y	6	1600	3782
V47D	0.09	24	3500
V47N	0.46	27	17000
Y48F[b]	0	—	—
Q49R	0.99	23	43000
K77M[b]	0	—	—
H110A[b]	0.07	84000	0.9
F121E	0.92	48	19000

[a] All kinetic constants measured with DL-glyceraldehyde as substrate. [b] Values for WT, Y48F, K77M and H110A from Bohren *et al.* (*S8*) . [c] Values for W20Y from Hohman *et al.* (*S10*)

Table S2: Vibrational frequencies of IDD743 bound to hALR2 mutants[a].

	$\bar{\nu}_{obs\ CN}$ (cm^{-1})[b]	$\Delta\bar{\nu}_{obs\ CN}$ (cm^{-1})[c]
wild-type	2241.6	—
W20Y	2240.9	-0.7
V47D	2240.0	-1.6
V47N	2238.5	-3.1
Y48F	2240.2	-1.4
Q49R	2241.2	-0.4
K77M	2239.4	-2.2
H110A	2242.1	+0.5
F121E	2240.7	-0.9

[a] All spectra were obtained at room temperature in 20 mM phosphate buffer (pH = 7.0).

[b] Frequencies were obtained by fitting the sum of at least three independent spectra.

[c] Change in frequency relative to wild-type.

Table S3. Predicted change in field along nitrile bond of IDD743 relative to wild-type[a].

Group 1[b]		Group 3[d]		Group 4[e]					
Mutant	$\Delta F_{\|\|}$[f]	Mutant	$\Delta F_{\|\|}$[f]	Mutant	$\Delta F_{\|\|}$[f]	Mutant	$\Delta F_{\|\|}$[f]	Mutant	$\Delta F_{\|\|}$[f]
W20Y	0.63	K21A	-0.24	A45D	-0.90	W79D	-1.04	F121A	-0.11
Y48F	0.07	D43A	0.30	A45N	0.25	W79F	0.45	F121D	0.28
K77M	-0.55	E51A	0.15	A45S	0.03	W79H	0.67	**F121E**	0.42
H110A	0.02	E53A	-0.01	H46A	-0.10	W79K	2.67	F121H	-0.08
		K77A	-0.53	H46D	-0.15	W79Y	-0.04	F121K	-0.05
Group 2[c]		K94A	0.01	H46F	-0.07	C80A	0.00	F121R	0.06
H46A	-0.10	D98A	0.00	H46H	-0.05	C80D	-0.61	F121S	-0.22
Q49G	-0.09	K116A	0.02	H46K	-0.08	C80S	-0.05	F121Y	-0.06
C80N	-0.05	K119A	0.00	H46N	-0.03	T81D	-0.10	L124D	0.03
C298I	0.01	E120A	-0.13	H46S	-0.11	T81V	0.02	L124E	0.03
S302R	0.04	D216A	0.10	V47A	-0.01	Y82D	-0.09	L124H	0.01
C303D	-0.36	R217A	-0.05	**V47D**	-3.86	Y82F	-0.01	L124K	-0.04
T304A	0.00	K262A	-0.06	V47H	-0.32	Y82H	-0.02	L124R	-0.04
S305G	0.00			V47K	2.30	Y82K	-0.04	L124S	-0.01
K307P	-0.03			**V47N**	1.39	F115D	-0.04	L124T	-0.01
D308L	0.04			V47S	-0.71	F115H	0.06	S302A	0.01
				Q49A	-0.09	F115Y	-0.01	S302C	0.01
				Q49E	0.18	K119A	0.00	S302D	0.00
				Q49H	-0.08	K119D	0.18	S302E	0.02
				Q49K	-0.21	K119R	0.18	S302K	0.01
				Q49R	-0.52	K119S	0.00	S302R	0.02
				Q49S	-0.08	E120A	-0.13	C303A	-0.04
				N50A	0.00	E120K	-0.17	C303D	-0.36
				N50D	-0.14	E120Q	-0.10	C303S	-0.03
				N50S	0.00	E120R	-0.19		

[a] Mutants chosen for infrared experiments in bold. [b] Previously reported mutations. [c] hALR2 to hALR1 mutations. [d] Charged residues within 15 Å of IDD743 nitrile. [e] Residues within 10 Å of IDD743 nitrile excluding W20, K21, Y48, H110, W111, T113, F122, P123, P218, W219, A299, L300. [f] Change in projection of field along nitrile bond (Mutant - WT) in kT/eÅ (1 kT/eÅ = 2.57 MV/cm at 298 K).

Supplemental References

S1. S. S. Andrews, S. G. Boxer, *J. Phys. Chem.* A **104**, 11853 (2000).

S2. S. S. Andrews, S. G. Boxer, *Rev. Sci. Instrum.* **71**, 3567 (2000).

S3. S. S. Andrews, S. G. Boxer *J. Phys. Chem.* A, **106**, 469 (2002).

S4. I. T. Suydam, S. G. Boxer, *Biochemistry* **42**, 12050 (2003).

S5. V. Lamour *et al.*, *Acta Crystallogr.* **55**, 721 (1999).

S6. C. E. Grimshaw, K. M. Bohren, C. J. Lai, K. H. Gabbay, *Biochemistry* **34**, 14366 (1995).

S7. K. M. Bohren, J. L. Page, R. Shankar, S. P. Henry, K. H. Gabbay, *J. Biol. Chem.* **266**, 24031 (1991).

S8. K. M. Bohren *et al.*, *Biochemistry* **33**, 2021 (1994).

S9. C. E. Grimshaw, K. M. Bohren, C. J. Lai, K. H. Gabbay, *Biochemistry* **34**, 14374 (1995).

S10. T. C. Hohman *et al.*, *Eur. J. Biochem.* **256**, 310 (1998).

S11. A. Podjarny, R. E. Cachau, T. Schneider, M. Van Zandt, A. Joachimiak, *Cell. Mol. Life Sci.* **61**, 763 (2004).

S12. E. I. Howard *et al.*, *Proteins Struct. Funct. Bioinform.* **55,** 792 (2004).

S13. T. Ehrig, K. M. Bohren, F. G. Prendergast, K. H. Gabbay, *Biochemistry* **33**, 7157 (1994).

S14. S. C. Lovell *et al.*, *Proteins Strut. Funct. Genet.* **50**, 437 (2003).

S15. N. Muzet, B. Guillot, C. Jelsch, E. Howard, C. Lecomte, *Proc. Natl. Acad. Sci. U.S.A.* **100**, 8742 (2003).

S16. W. L. DeLano, http://www.pymol.sourceforge.net

S17. O. Elkabbani *et al.*, *Acta Crystallogr* **50**, 859 (1994).

S18. W. Rocchia, E. Alexov, B. Honig, *J. Phys. Chem.* B **105**, 6507 (2001).

S19. K. Sharp, B. Honig, *Chemica Scripta* **29A**, 71 (1989).

S20. D. Sitkoff, K. a. Sharp, B. Honig, *J. Phys. Chem.* **98**, 1978 (1994).

S21. N. Holmberg, U. Ryde, L. Bulow, *Protein Eng.* **12**, 851 (1999).

S22. M. J. Frisch *et al.*, http://www.gaussian.com.

S23. http://dasher.wustl.edu/tinker/.

S24. S. J. Weiner *et al.*, *J. Am. Chem. Soc.* **106**, 765 (1984).

S25. D. Bashford, D. A. Case, *Annu. Rev. Phys. Chem.* **51**, 129 (2000).

S26. C. D. Snow, E. J. Sorin, Y. M. Rhee, V. S. Pande, *Annu. Rev. Biophys. Biomol. Struct.* **34**, 43 (2005).

S27. M. K. Gilson, B. H. Honig, Biopolymers **25**, 2097 (1986).